



Universiteit
Leiden
The Netherlands

On the interactions between carbohydrates and immune cells

Steuten, K.

Citation

Steuten, K. (2026, July 2). *On the interactions between carbohydrates and immune cells*. Retrieved from <https://hdl.handle.net/1887/4307272>

Version: Publisher's Version

License: [Licence agreement concerning inclusion of doctoral thesis in the Institutional Repository of the University of Leiden](#)

Downloaded from: <https://hdl.handle.net/1887/4307272>

Note: To cite this publication please use the final published version (if applicable).

Chapter 3

Correlating mannose binding to myeloid cell function

Kas Steuten¹, Johannes J.A. Bakker¹, Ward Doelman¹, Diana Torres-García¹, Amit Cherian¹, Christian Kurts³, Roger Riera², Lorenzo Albertazzi² & Sander I. van Kasteren¹

¹ Department of Chemical Biology and Immunology, Leiden Institute of Chemistry, Leiden, The Netherlands

² Department of Biomedical Engineering and Institute for Complex Molecular Systems, Eindhoven University of Technology, Eindhoven, the Netherlands

³ Institute of Experimental Immunology, University of Bonn, Bonn, Germany

Parts of this chapter are published as: Steuten, K. *et al.*, *Nature Communications*, 17, 886 (2026).

3.1 Introduction

Myeloid immune cells such as dendritic cells (DCs) and macrophages are key sentinels of the immune system. They sense the presence of microbial species or altered self through pattern recognition receptors (PRRs), which in turn can trigger innate and adaptive immune responses. One important family of PRRs are the carbohydrate-binding proteins of the C-type lectin receptor family (CLRs).^{1,2} CLR ligation can induce various immune functions, including endocytosis, polarization, cytokine secretion, cell adhesion, and motility, which can subsequently trigger downstream immune responses.^{2,3}

One receptor which is archetypal in its biological complexity is the mannose receptor (CD206, MR). This lectin is expressed on cells of the myeloid lineage⁴⁻⁶, where it carries out a variety of functions. It acts as an endocytic receptor to clear soluble glycoproteins and as a phagocytic receptor of glycosylated particles leading to clearance and antigen presentation.⁷⁻⁹ It also acts as a mediator of inflammatory signaling by inducing M2 polarization of macrophages and inducing T cell tolerance.^{10,11} How the MR translates ligand recognition to all these separate functions remains unknown. Structurally, the MR contains multiple functional domains, including an N-terminal cysteine-rich domain capable of binding sulfated glycans (that can inhibit receptor function¹²), a fibronectin-like domain capable of binding collagen peptides^{13,14}, and eight C-type lectin domains (CTLs), of which only CTL4 and CTL5 exhibit functional calcium-dependent binding of neutral sugars.¹⁵ These domains are further modulated by glycosylation at seven N-linked sites, influencing receptor binding properties.¹⁶ The intracellular tail lacks classical signaling motifs^{7,17}, though recent evidence suggests phosphorylation and diaromatic motifs may facilitate endosomal sorting and signaling.¹⁸⁻²⁰

Despite this biological complexity, the MR has been under heavy investigation as vaccine targeting receptor. Ligation of the MR was shown to lead to the enhanced cross-presentation (and thus cytotoxic CD8 T-cell activation) of glycoprotein antigens, which can be employed to enhance the anti-cancer and anti-viral properties of therapeutic vaccines.^{21,22} However, further pursuit of this phenomenon has led to conflicting results.²³⁻³⁰ No studies have yet managed to correlate the binding of specific ligands to the MR to downstream biology (i.e., uptake and/or cross-presentation). For example, bulk methods such as surface plasmon resonance (SPR) or flow cytometry, failed to correlate binding affinities with uptake or cross-presentation, highlighting the need for methodologies capable of quantifying receptor-ligand kinetics in the native cellular context.^{24,31}

Here, we present the correlation of mannose binding kinetics with cellular function using the Glyco-PAINT-APP developed in **Chapter 2**, such that we can obtain binding parameters of glycans to the MR on myeloid cells. We developed a probe library in which the probes contained a cross-presentable epitope between the glyco-clusters and

fluorophore. This allowed us to quantify lectin binding kinetics and correlate this with uptake, and cross-presentation of the same construct. Correlating the binding kinetics to uptake and cross-presentation, yielded unexpected findings that challenge current understanding of MR biology. We found that the binding of the glyco-clusters was very heterogeneously distributed over the surface of the DCs. On a single cell, highly varying binding regions were observed: from areas with no probe binding, to regions with low numbers of binding events to a highly mobile MR, to unique sub-cellular population of areas where probes engaged with the cell surface in an MR-independent manner. We found a strong negative correlation (Pearson's R: -0.90) between these highly mobile receptors and probe endocytosis by the DC, which was highly MR-dependent. In contrast, cross-presentation of mannosylated antigens showed a strong positive correlation only to the residence time τ of the specific probe on DCs of both WT and MR^{-/-} origin (Pearson's R: 0.82 and 0.77 respectively). In a second application of the approach, we could also quantify changes in mannoside binding during the macrophage polarization trajectory and found that the cumulative duration of individual binding events was enhanced for the M2 phenotype in accordance with upregulated MR expression and endocytosis of ligands.

3.2 Results

3.2.1 Uptake and antigen presentation of SLP glycoforms

In **chapter 2** we demonstrated the quantification of on-cell kinetic parameters of mannose ligands binding to BMDC using Glyco-PAINT-APP. To evaluate whether these parameters could be predictive for some of the previously reported roles (see introduction) of the MR and related CLRs on BMDCs, we set out to incorporate a functional element in the glycan clusters. We therefore designed Synthetic Long Peptide (SLP) versions of the fluorophore-labelled mannose clusters that also contained the model cross-presentable epitope Ovalbumin₂₆₃₋₂₇₅ (OVA SLP). Uptake of this epitope by dendritic cells can lead to presentation on H2-kb MHC-I alleles and subsequent activation of cytotoxic T cells in a process called antigen cross-presentation.³² It has been hypothesized that long-peptide variants are more effectively cross-presented and that different glycoforms of these SLPs show varying cross-presentation behavior.^{26,33,34} The antigenic cargo would allow us to monitor the various binding parameters (by Glyco-PAINT-APP) but also uptake (by flow cytometry), and antigen cross-presentation (using the cognate OT-I T-cell), thus having readouts for these three aspects of MR biology from a single probe.

The constructs were synthesized using in-line solid-phase peptide synthesis of the peptide antigen and an oligo-azidolysine (6-azidonorleucine) cluster, followed by on-resin modification with fluorophore. Copper-catalyzed azide-alkyne cycloaddition (CuAAC)-mediated^{35,36} coupling of the mannose glycans to the azidolysine clusters

3.2. Results

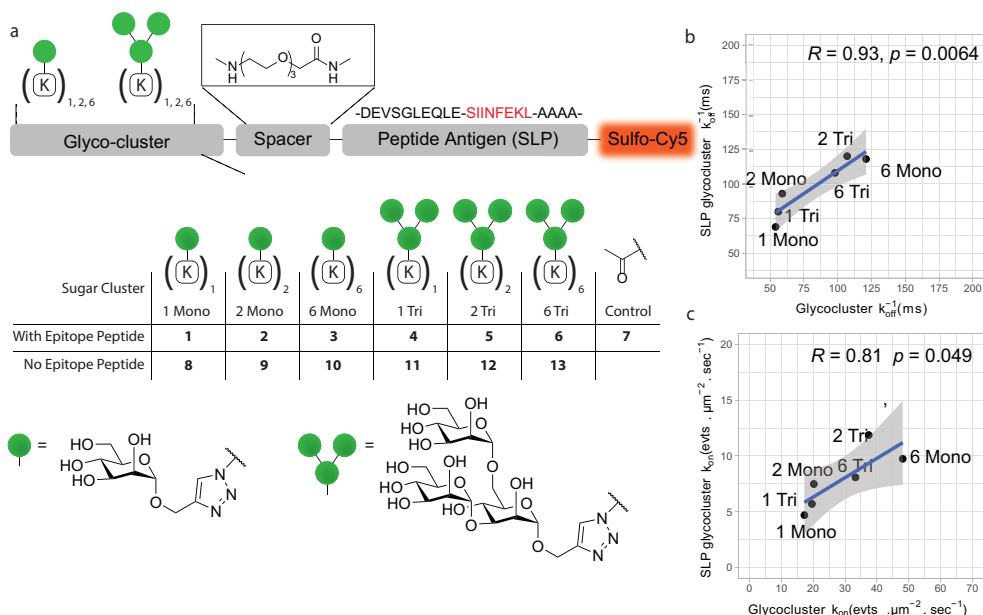


Figure 3.1: Fluorescently labelled mannose ligands with SLP antigenic peptide retain MR-binding (a) Design of synthetic glycoclusters. 1-7 carry an N-terminal long peptide from Ovalbumin₂₆₃₋₂₇₅ and a sulfo-Cy5 fluorophore on a C-terminal lysine side chain. Glycocluster series 8-13 do not contain this SLP but are directly attached to an ATTO655 fluorophore. (b, c) Correlation analysis of the median rel. k_{on} and k_{off}^{-1} between probes with identical glycan but bearing long peptide antigens binding to CHO-MR cells. Data points are medians for all squares analysed with a 20×20 grid and filtered with Density_Ratio > 2, R_Squared \geq 0.9, and Nr_Tracks/Square > 20. Pearson's R and two-tailed t test P value are displayed in the correlation plots.

in solution yielded the target glycosylated SLPs. This resulted in mono-, bi- and hexavalent versions of mono- (1-3) or trimannosylated (4-6) SLPs and a non-glycosylated control molecule (7) that are displayed in **Figure 3.1a** (synthetic procedures and characterization are not part of this thesis, an overview of the conversions can be found in **Figure S3.1**). These glycan motifs span a K_D range for MR-binding from $3 \mu\text{M}$ to more than $100 \mu\text{M}$ (based on SPR studies using recombinant receptor^{4,31}), thereby enabling investigation of glycan-structure-binding-activity relationships over a large affinity range. To verify the absence of artefacts resulting from the SLP antigenic cargo on kinetics, we next compared the median on- and off-rates of OVA SLP 1-6 to glycoclusters 8-13 that lack the peptide on CHO-MR cells and plotted the correlation between the two (**Figure 3.1b, c**). Neither extension of the peptide core, nor the change of the fluorophore from ATTO655 to sulfo-Cy5, significantly affected k_{off}^{-1} . A decrease in the median number of binding events per square (rel. k_{on}) was detected for the glycan SLPs with respect to the glycans 8-13, potentially originating from altered

physical-chemical properties of the peptide cargo.

The binding parameters of these glycosylated SLPs were assessed for their binding to live WT BMDCs and BMDCs derived from MR^{-/-} mice. This analysis enabled us to precisely determine the contribution of glycan SLP binding events mediated by the MR, and not by any of the other lectins present on the DCs. It was observed that a population of squares engaging in binding events with 2-dimensional surface mobility (diffusion coefficient) and low event density (k_{on}) was uniquely present for the WT cells that were not observed on DCs lacking MR (**Figure 3.2a, b**). This population of binding events appeared most prominent for glycan SLPs **2, 3** and **6** but not for **1, 5** and **7**. It was also assessed whether internalization of the probes and resulting removal of a ligand from the TIRF-plane, affected track length. Cells were therefore treated with the uptake inhibitor Cytochalasin D (CytD, which works through inhibition of actin polymerization).^{37,38} Event density, dwell time τ and diffusion coefficient all increased significantly for probes 1 Tri (**4**) and 2 Tri (**5**) after CytD treatment of BMDC (**Figure S3.2** for probe pairwise comparisons, **Figure S3.3a, b** for comparisons between WT, MR^{-/-} and CytD conditions, with **Table 3.1** listing numeric values). Together, these data suggest that the internalization of the MR is an important parameter to consider for cell surface binding properties.

Next, uptake of the SLP library was measured by incubating BMDCs with SLP **1-7** for 1 h, followed by quantification of the sCy5 signal by flow cytometry. These data showed that a specific subpopulation of MR⁺CD11c⁺ DCs (**Figure 3.2c, Figure S3.5b, e** show high MR-mediated uptake (**Figure S3.5d**, for competition with broad-spectrum ligand mannan and **Figure S3.4a, b** for intracellular localization of SLP **5** and **6**), highlighting the intrinsic heterogeneity of these cells. Quantification of this effect using phagocytic index (PI)³⁹ revealed a glycoform-specific profile with divalent trisaccharide-modified SLP **5** being most effectively taken up in contrast to its hexavalent counterpart **6**. Uptake of the non-glycosylated control **7** was at near-baseline levels, emphasizing the glycan-mediated engagement of endocytic lectins. Similarly, all uptake was abolished MR^{-/-} cells (**Figure S3.5b**).

The cross-presentation efficiency of these glycosylated SLPs was tested next by pulsing BMDCs (pretreated for 2 hours with TLR4 ligand MPLA) with 40 nM SLP (which is in a similar concentration range as Glyco-PAINT binding studies, see **Figure S3.4c, d** for different antigen dosages and alternative quantification of CFSE dilution in proliferating T cells) for 2 hours followed by a 3-day coculture with CD8⁺ T cells that were freshly isolated from OT-I mice. The non-mannosylated control SLP **7** was most efficiently cross-presented whereas SLPs decorated with mannosides of increasing complexity and valency **1-6** showed an unexpected decrease in T-cell proliferation induction. We also evaluated the cross-presentation efficiency in MR^{-/-} cells and found an identical glycoform-dependent pattern. To validate correct differentiation and functional response of the MR^{-/-} cells as compared to WT cells we characterized the change in cell surface marker expression levels in response to LPS stimuli

3.2. Results

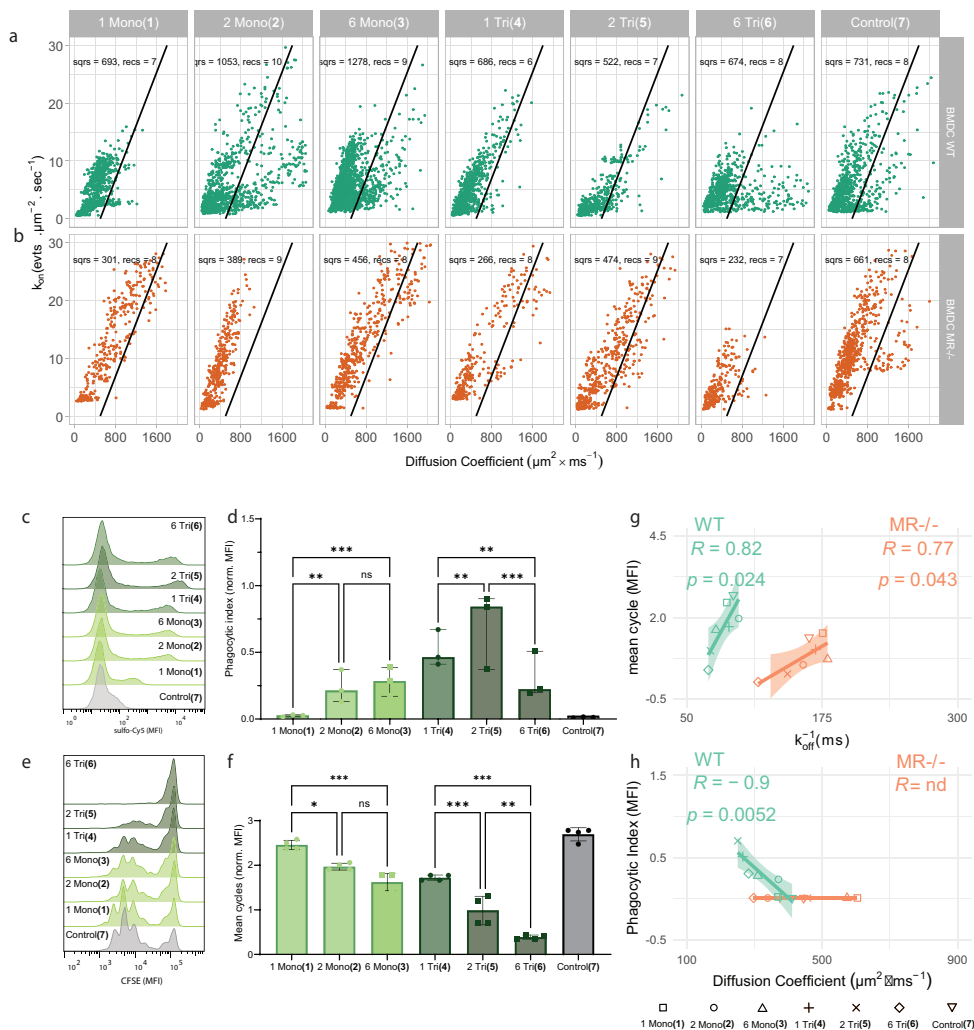


Figure 3.2: Unique population of MR-specific binding events and kinetic parameters correlate with ligand functionality. (a) Scatterplots of the rel. k_{on} and diffusion coefficient per square for binding events between probes 1-7 and WT BMDC. Number of accepted squares and recordings are written in the plots; the diagonal black line represents a manually drawn gate that identifies MR-mediated binding events in WT cells. (b) Same as in a for MR^{-/-} BMDC. (c) Histograms of BMDCs incubated with probe 1-7 for 1 h and subsequent measurement of endocytosis in CD11c⁺ cells using flow cytometry. (d) Bar chart of c as the phagocytic index. (e) Histograms of CFSE dilution in dividing OT-I T cells that were cocultured for 3 days with mature BMDC that were pulsed for 2 h with antigens 1-7 and measured using flow cytometry. (f) Bar chart of the average number of cell divisions per T cell obtained from e. (g) Correlation between median k_{off}^{-1} for WT or MR^{-/-} BMDCs and the mean number of T-cell divisions. (h) Correlation between probe median diffusion coefficients for WT or MR^{-/-} cells and phagocytic index. Glyco-PAINT-APP analysis was done using a 20×20 grid and filtered with Density_Ratio > 2, R_Squared \geq 0.9, and Nr_Tracks/Square > 20. Pearson's R and two-tailed t test *P* value are displayed in the correlation plots.

and found no aberrant expression patterns (**Figure S3.5a**). Additionally, we verified DC origin (see **Figure S3.4f** for steady-state cross-presentation of antigens in splenic DCs²⁶) and the effect of timing of DC maturation and found an identical pattern for all timepoints in agreement with the observed diminishing effect of antigen mannosylation on T cell proliferation (**Figure S3.4e, f**).

Having observed this non-linear (**Figure S3.6a**) and, to us at least, counter-intuitive relationship between binding, endocytosis, and MHC-I-restricted cross-presentation, we next determined whether any of the subcellular kinetic parameters of SLP binding to DCs was predictive of either of these biological functions. A correlation was made using the median values of the following 8 kinetic parameters as derived by Glyco-PAINT-APP per analysed square (see also **Table 2.1**): τ (ms), rel. k_{on} ($\text{events} \cdot \text{s}^{-1} \mu\text{m}^{-2}$), total track duration (s), long track duration (top 10%, s), short track duration (bottom 10%, s), diffusion coefficient D ($\mu\text{m}^2 \text{s}^{-1}$), mean speed ($\mu\text{m} \text{s}^{-1}$), and maximum speed ($\mu\text{m} \text{s}^{-1}$). From this analysis, glycan-SLP residence time (τ) on the DC surface was the best predictor for cross-presentation and this correlation upheld for the MR^{-/-} cells. Furthermore, high diffusion coefficients (and accordingly larger displacement of the track) correlated with low uptake of the SLP (**Figure 3.2g, h**). Both correlations were disrupted after cell treatment with CytD (**Figure S3.6b**). These observations imply a mechanism where binding events of long duration and high on-membrane mobility are less likely to result in receptor-mediated endocytosis but more likely to enter a cytosolic cross-presentation pathway. Taken together, the correlations between on-cell kinetics and cellular functionality demonstrate the potential of the Glyco-PAINT-APP to uncover functional glycan-structure-activity relationships.

3.2.2 MR binding on macrophages

Thus far we have found strong discrepancies in detected glycan binding parameters in the CHO-MR overexpression system versus native lectin-expressing cells. We next studied whether such discrepancies also extended across different myeloid cells. For this, we studied the changes in carbohydrate binding upon macrophage polarization. Certain pro- and anti-inflammatory stimuli are known to affect absolute levels of the MR on the cell surface upon polarization of the macrophage from its 'naïve' M0-like state to either the inflamed M1-like or wound-healing M2-like phenotype.⁴⁰ It is, however, not known whether this change in MR (and related CLR)-levels also alters binding preferences of the macrophage. We attempted to investigate this by quantifying the binding parameters of mono- and hexavalent mono- and trimannoside **8**, **10**, **11** and **13** MR ligands respectively to murine bone marrow-derived macrophages (BMDMs) treated with either M1 inducing (LPS and IFN γ), M2-inducing (IL-4) stimuli or left untreated for M0 (**Figure 3.3a, c**). Here we observed a glycoform-specific trend with increased binding for the hexavalent clusters in comparison to the monovalent clusters

3.2. Results

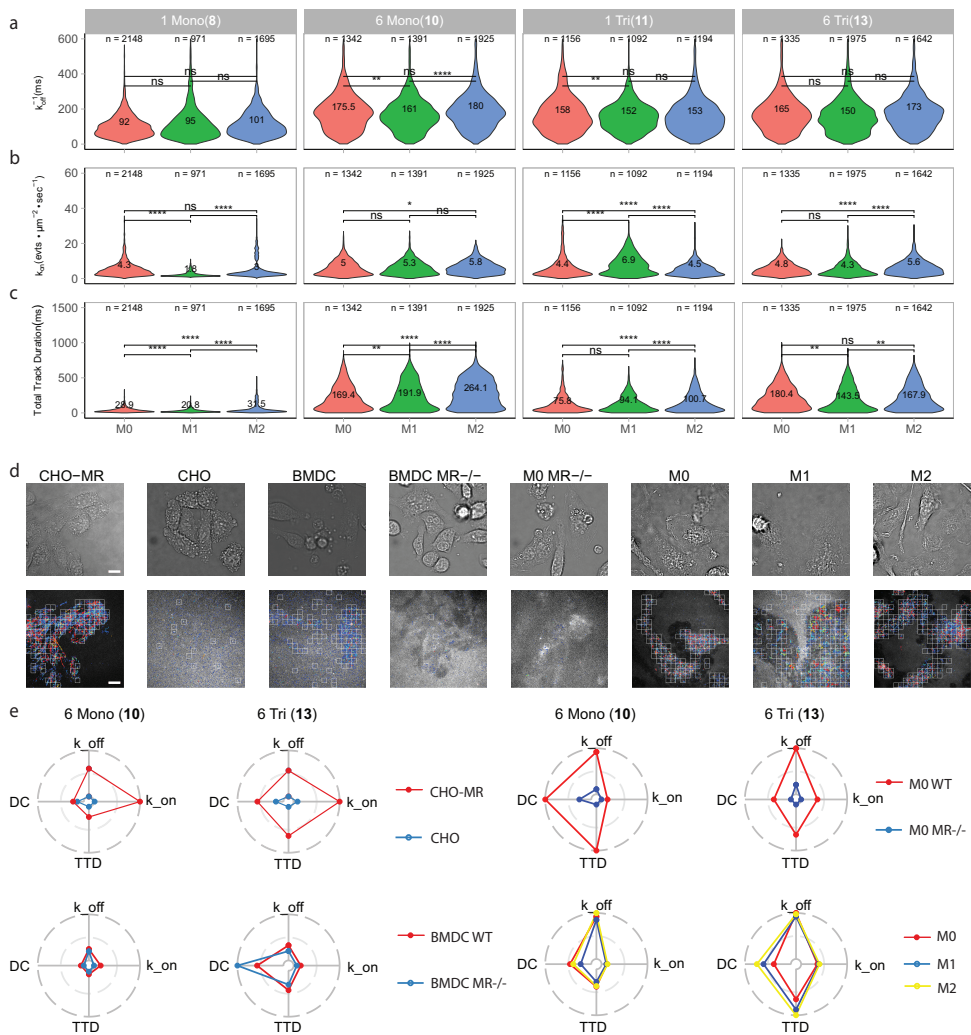


Figure 3.3: Mannose glycan binding characteristics are highly dependent on lectin expressing cell. (a-c) Violin distribution k_{off}^{-1} , rel. k_{on} and total track duration respectively of glycans **8**, **10**, **11** and **13** on M0, M1 or M2 polarized macrophages. (d) Representative examples of brightfield images (top row) and track reconstructions (bottom row) of hexavalent trimannoside **13** binding to all cell types that were evaluated in this study. (e) Radar plots summarizing four normalized kinetic parameters for glycan **10** and **13** for the various combinations of cell types. n, indicates the number of squares from which the data were obtained. Glyco-PAINT-APP analysis was done using a 20×20 grid and filtered with Density_Ratio > 2 , R_Squared ≥ 0.9 , and Nr_Tracks/Square > 20 (for BMDC recordings R_Squared ≥ 0.1). Significance was assessed using two-way ANOVA followed by a Tukey post-hoc test. Tracks in (c) are coloured from short to long track length (light blue to red). Abbreviations in panel (e) DC: Diffusion Coefficient, TTD: Total Track Duration, k_{on} rel. k_{on} , k_{off} : k_{off}^{-1} . Displayed scalebars in CHO-MR images in **d** represent $10 \mu m$ and are identical for each image.

much alike the CHO-MR binding distribution (**Figure S2.4b, c**). Additionally, the detected binding events were also resulting in endocytic glycan uptake as determined by flow cytometry where the M2 macrophages appeared to be more endocytic (**Figure S3.7a, b**). Surprisingly, a uniform increase in number of binding events (rel. k_{on}) across all glycans upon M2 polarization, which is known to upregulate MR expression levels⁴¹, was not apparent from these data. However, for the total binding as quantified by the total track duration (number of events multiplied with their duration) within a square, there appeared to be a vast increase for the M2 phenotype compared to M0 and M1 (**Figure 3.3c**) for all glycans except **13** (when square selection criteria were adjusted to $R_Squared > 0.1$ to accommodate long duration binding events, as illustrated in **Figure S3.8a, c**). This suggests the emergence of a distinct population of long duration binding events that are potentially the result of CLR upregulation by M2 macrophages, analogous to increase in highly mobile long tracks that were seen to be MR-specific on DCs. To evaluate effects of polarization on the spatial clustering of binding events, a clustering analysis was performed using the x, y coordinates of each track. This analysis did not result in glycoform-specific trends for clustering of events on macrophage cell surface (**Figure S3.7c**). Next, binding data for polarizing macrophages were pooled with the previously acquired binding data on CHO, CHO-MR, BMDC WT, BMDC MR^{-/-} and BMDM MR^{-/-} to precisely evaluate the contribution of MR-mediated binding events in a single analysis. In **Figure 3.3d** representative examples of recordings with **13**-binding events are shown and in **Figure 3.3e** the relative contributions of four main kinetic parameters are visualized in radar plots for the combinations of MR-expressing or MR-lacking cell types, and BMDM polarization states. From these plots it is apparent that indeed the majority of **10** and **13** binding events detected on CHO-MR and BMDM are MR-mediated. This contrasts with BMDC, for which there seems to be the highest degree of redundancy in non-MR binding partners.

3.3 Discussion and conclusion

In this work we demonstrate the correlation of live-cell kinetic parameters that were obtained with the Glyco-PAINT-APP-approach, to receptor functions such as uptake and cross-presentation, which had been the subject of much controversy. The wealth of binding and receptor-ligand information obtained by this approach – which had previously thwarted correlation of bulk binding parameters to function - led us to identify key parameters of the interaction that could be predictive of uptake and cross-presentation behaviour: the presence of regions with very long ligand residence times (τ) correlated with cross-presentation ability, and the lack of ligand movement of the receptor with internalisation. This – combined with the fact that uptake efficiency and cross presentation showed no correlation – suggests that multiple processes are

3.4. Methods

likely taking place on the cell surface, either mediated by other lectins, or perhaps simply the macropinocytosis of which DCs display a phenomenal rate: they can internalize their entire cell membrane in about half an hour, or the equivalent of a cell volume in an hour.^{42,43} Watts and co-workers have shown macropinocytosis to be a key mechanism for inducing antigen cross-presentation.^{44,45} We propose the hypothesis that the increased dwell time τ on the surface of a DC – either through receptor mediated interaction or through α -specific interactions – increases the chance of an antigen being internalized in a macropinosome. At the same time, the binding of a ligand to a clathrin-anchored MR increases its chance of internalization into a non-cross presentation enabled vesicle. We do, however, need to emphasize that the observed correlations do not by any means imply a causal relationship. To further explore this causality, experiments with different SLP antigens or genetic knockouts of proteins other than CLR_s involved in the endocytosis pathway, could be designed. Our proposed model would, however, explain some of the other reports of non-linear uptake-cross-presentation relationships for mannosylated SLPs^{23–25} and potentially even for antibody-antigen conjugates.⁴⁶

3.4 Methods

Acknowledgments Nico Meeuwenoord and Hans van Elst are acknowledged for their assistance with HPLC and SEC purifications. We thank the Flow Cytometry Core Facility (FCF) of Leiden University Medical Center (LUMC) in Leiden, The Netherlands for experimental support, use and maintenance of BD Fortessa I and Sony ID7000. We thank the Animal Research Facility (ARF) and Bram Slütter at the Leiden University Faculty of Science for mouse breeding and colony management.

Ethical Statement All animal experiments received approval from the Dutch Central Authority for Scientific Procedures on Animals (CCD) on license number AVD1060020198832 and were conducted in accordance with the European Union Directive 2010/63/EU, recommendation 2007/526/EC.

Data and code availability Representative raw recordings and all processed tracking data have been deposited in the Zenodo repository under DOI:

<https://doi.org/10.5281/zenodo.17485662>

Mice Male C57Bl/6J and OT-I (C57BL/6-Tg(Tcr α Tcr β)1100Mjb/J) mice were purchased from Charles River Laboratory. MR^{-/-} mice on a C57BL/6J background were originally provided by Nussenzweig.⁴⁷ The animals were provided with water and food *ad libitum* under a 12:12 day/night cycle. Mice ranging from 8 to 15 weeks

old were euthanized by cervical dislocation before harvest of lymphoid organs and/or thigh bones, femur, and tibia.

3.4.1 Cell culture

Bone marrow-derived dendritic cells (BMDC) Bone marrow (BM) was isolated from femurs, tibias, and thigh bones of WT or MR^{-/-} C57Bl/6J mice via centrifugation (1900 rcf, 4.5 min) of scissor-cut bones that were placed inside a standard 200 μ L micropipette tip in a 1.5 mL tube. The resulting pellet was subjected to red blood cell (RBC) lysis by resuspending in 0.5 mL of ammonium chloride-potassium (ACK) lysis buffer (Gibco, A1049201). After 3 min incubation at room temperature, the suspension was filtered over a 70 μ m filter (Falcon, 352350), rinsed with 5 mL PBS and washed once with PBS by 5 min centrifugation at 300 rcf at room temperature. Thus obtained BM was cryopreserved in 10%DMSO in FCS according to standard methods⁴⁸ or directly resuspended at 1×10^6 cells/mL in 15 cm uncoated culture dishes (Sarstedt, 82.1184.500) in complete RPMI-1640 (Capricorn, RPMI-A) supplemented with 10% heat-inactivated fetal calf serum (FCS, Gibco, A5670701), penicillin (100 I.U./mL) and streptomycin (50 μ g/mL) (Gibco, 15140148), 2 mM GlutaMAX (Gibco, 35050061), 50 μ M 2-mercaptoethanol (Gibco, 31350010) and 20 ng/mL mGM-CSF (Peprotech, 315-03) and cultured in a humidified incubator at 37 °C and 5% CO₂. On day two, 5 mL of fresh medium was added and on day four cells were reseeded in fresh medium at 1×10^6 /mL. Cells were used for microscopy and T cell activation experiments on day 7 or 8.

CHO-MR cells The CHO-MR cell line was kindly provided by Luisa Martinez-Pomares⁴⁹ and cultured in DMEM/F12 without phenol red (Gibco, 21041025), supplemented with 10% FCS, penicillin (100 I.U./mL), streptomycin (50 μ g/mL), and selection antibiotic G418 (0.6 mg/mL). A layer of adherent cells was washed with PBS and cells were harvested by 10 min incubation with 2 mM EDTA in PBS and subcultured approximately twice per week at a 1:5 split when cells reached 70–80% confluency.

3.4.2 Statistical analysis and sample size

Statistical analyses were conducted to compare glycan ligand binding kinetics across probes using the Glyco-PAINT square-based subsampling technology. Subsampling subcellular regions (squares) within fields of view increased the number of independent data points, enhancing statistical power compared to treating entire fields of view or cells as single units. For all Glyco-PAINT experiments at least 3 biological replicates (independent experiments with fresh mouse material or new passage number for cell lines) with 3 technical replicates (fields of view per condition) were recorded. For

3.4. Methods

flow cytometry assays at least 3 biological replicates with 2 technical replicates per condition were conducted. A two-way ANOVA was used to assess differences among probes with respect to kinetic parameters derived from Glyco-PAINT experiments and flow cytometric assays, followed by Tukey's Honest Significant Difference (HSD) test for post-hoc comparisons to control Type I error. Significance is reported as: $p \geq 0.05$ (not significant, ns); $p < 0.05$ (*); $p < 0.01$ (**); $p < 0.001$ (***); and $p < 0.0001$ (****).

3.4.3 Functional Assays

Fluorescent glycan probes Glycan and glycan SLP probes were stored as lyophilized powders at -20°C . Upon thawing, vials were reconstituted in DMSO and concentration was determined by measurement of absorbance using Nanodrop apparatus with extinction coefficients $\text{eCy5} = 250.000 \text{ M}^{-1}\text{cm}^{-1}$ at 641 nm and $\text{eATTO655} = 125.000 \text{ M}^{-1}\text{cm}^{-1}$ at 663 nm. Small aliquots were stored at -20°C until use. Synthetic procedures and characterization of SLPs **1 - 7** is described in Doelman *et al.*⁵⁰ Additionally, a synthetic scheme can be found in **Figure S3.1**.

OT-I T cell isolation A 70 μm filter was placed on a 50 mL tube and pre-wetted with PBS supplemented with 2 mM EDTA and 2% FCS (single-cell suspension buffer, SCSB). Freshly harvested spleens from OT-I transgenic mice were placed on the filter and disrupted with the back end of a syringe. After thorough washing, the suspension was centrifuged (10 min, 300 rcf, rt). Next, the pellet was gently resuspended in 2 mL of ACK lysing buffer (Gibco, A1049201). After 3 min incubation the suspension was diluted with 10 mL PBS, filtered once more, and centrifuged again (300 rcf, 10 min, rt). The pellet was resuspended and subjected to magnetically-activated depletion of non-target cells using the "Naïve CD8a+ T cell isolation Kit" (Miltenyi, 130-096-543) according to the manufacturer's protocol. The obtained T cells were counted and resuspended at a density of $1 - 15 \times 10^6$ cells / mL in 1 mL PBS with 5 μM CFSE (Biolegend) and incubated for 15 min at 37°C . After incubation, cells were spun down (10 min, 300 rcf, rt), washed once more with complete RPMI-1640 and were ready for downstream use.

Splenic DC isolation Spleens isolated from C57Bl/6J mice were placed on a 10 cm petri dish (Sarstedt, 83.3902) containing 5 mL HBSS (Gibco, 14025092) supplemented with 1 mg/mL collagenase IV (Sigma, NC2115693) and 20 U/mL DNase (Thermo Scientific, EN0525) and minced into small pieces. After incubating for 30 min at 37°C , tissue digestion was stopped by addition of 2 mM EDTA. The remaining homogenate was disrupted and RBC-lysed as described above and subjected to magnetically-activated depletion of non-target cells using the "Pan Dendritic Cell isolation Kit" (Miltenyi, 130-100-875) according to manufacturer's protocol.

Glycan uptake and cell surface staining 2.5×10^5 WT, MR^{-/-} BMDC or BMDM were seeded after treatment with polarizing stimulus as described below in a 96 well v-bottom plate (Sarstedt, 82.1583001). The next day, Glycan SLP probes were added to the cells at 250 nM and incubated for 1 h at 37 °C. Active uptake was halted by addition of ice-cold PBS and washed twice with PBS + 2% FCS + 2 mM EDTA (300 rcf, 5 min, rt). Cells were stained with a selection of the following stains and antibodies: Zombie Yellow (Biolegend, 423103, 1:500), TruStain FcX (Biolegend, cat no 101319, 1:100), CD11c - eFluor450 (clone: N418, eBioscience, cat no 48-0114-82, dilution 1:200), CD206-AF488 or AF647 (clone: MR5D3, Biorad, MCA2235A488T, 1:20), CD86-PerCP (Biolegend, cat no 105025, clone GL-1, 1:200), F4/80-APC-Cy7 (Biolegend, cat no 123117, clone BM8, dilution 1:400), MHC-II-AF488 (Biolegend, cat no 107615, clone M5/114.15.2, dilution 1:1000) for 30 min on ice. Then cells were washed twice with PBS + 2% FCS + 2 mM EDTA and acquired on Guava EasyCyte 12HT. For BMDM uptake and characterization, an identical procedure was followed but acquisition was performed on Sony ID7000 spectral flow cytometer. Analysis was performed using FlowJo v8. Phagocytic index (PI) was calculated according to the equation below. Statistical analysis and plotting were performed using GraphPad Prism.

$$PI = \left(\% sCy5^+ \cdot MFI_{sCy5^+} \right) - \left(\% sCy5^- \cdot MFI_{sCy5^-} \right)$$

Confocal imaging BMDC were cultured as described above and plated on IbidiTreat μ -Slide 8 Well High dishes (Ibidi, 80806) at 0.5×10^6 cells per well. Cells were incubated with Cy5-labeled SLP 250 nM for 1 h at 37 °C in complete RPMI. Following ligand incubation, cells were washed twice with ice-cold PBS and fixed incubated with CD11c-BV421 (BioLegend, cat no 117329, clone N418, dilution 1:100) antibody for 30 min on ice. Then cells were washed twice and incubated with 4% paraformaldehyde (PFA) in PBS for 15 min at room temperature. Fixed cells were permeabilized with 0.1% Triton X-100 in PBS for 20 min and blocked with and washed twice with blocking buffer (PBS + 2% FCS + 2 mM EDTA). Then cells were incubated with LAMP1-AF488 (BioLegend, cat no 121607, clone 1D4B, dilution 1:100) and EEA1-AF594 (MBL Life Sciences, cat no M176-A59, clone 3C10, dilution 1:100) antibodies for 1 h on ice. After final washes, coverslips were mounted in glycerol/DABCO mounting medium. Images were acquired using a Leica Stellaris 8 White Light Laser (WLL) confocal microscope equipped with a 63 \times /1.40 NA oil-immersion objective. Excitation was performed at 638 nm for Cy5, 488 nm for AF488 and 561 nm for AF594, with detection windows set according to manufacturer recommendations to avoid channel crosstalk. Line averaging (n = 2–4) and sequential scanning were applied where appropriate. All acquisition parameters (laser power, detector gain, pinhole size) were kept constant between conditions. Images were processed in LAS X software (Leica

3.4. Methods

Microsystems) and analyzed in Fiji (ImageJ) without nonlinear contrast adjustments.

T cell proliferation assay 5×10^4 BMDC or 1×10^5 splenic DC were seeded in 96 well Nunc U-bottom plates (Thermo Scientific, 168136) and pulsed with Glycan SLP at 40 nM for indicated time. In indicated experiments, DC were pretreated with 1 $\mu\text{g}/\text{mL}$ MPLA (Avanti, 699800P) for 2 h before antigen pulse. After antigen pulse was finished, the plate was spun down for 3 min at 600 rcf, washed once with complete RPMI-1640 and $1 - 1.5 \times 10^5$ freshly isolated, CFSE-stained OT-I T cells were added to the pulsed DCs in 200 μL complete RPMI-1640 and incubated at 37 °C. After 3d of coculture, the plate was spun down (3 min, 600 rcf, 4 °C) and supernatant was removed and stored at -80°C. Cells were washed with FACS buffer (PBS with 2 mM EDTA, 2% FCS and 7.4 mM NaN_3) and stained with Aqua Live/DEAD (Invitrogen, L34957, 1:500), TruStain FcX (Biolegend, 101319, 1:100), CD8a - APC (clone: 53-7.6, Biolegend, 100711, 1:200), and TCR V beta 5.1/5.2 - eFluor450 (clone: MR9-4, eBioscience, 48-5796-82) for 30 min on ice, washed two times and acquired on a BD Fortessa I flow cytometer and analyzed using FlowJo v8. To calculate mean cycle, the CFSE dilution factor was obtained by dividing the MFI of the antigen pulsed condition by the DMSO pulsed condition expressed as Log_2 .⁵¹ Statistical analysis and plotting was performed using GraphPad Prism v10.

BMDM polarization At day 6 adherent macrophages were harvested by aspiration of medium, washing once with PBS and incubation with 10 mL of 2 mM EDTA in PBS for 10 min at 37 °C. Cells were reseeded in complete medium with addition of polarizing stimulus, 20 ng/mL IFN- γ (Peprotech, 315-05-100UG) + 100 ng/mL LPS-EB (Invivogen, tlrl-ebllps) for M1 or 20 ng/mL IL-4 (Peprotech, 214-14-20UG) for M2 for 16 h.

3.4.4 Imaging and analysis

Glyco-PAINT optical setup Single-molecule imaging was performed on a Nikon Ti2 N-STORM system equipped with a TIRF module, Z piezo element, perfect focus system for axial drift correction and an OkoLab incubator with temperature and CO_2 controller (37 °C and 5% CO_2) for live-cell imaging. Recordings were acquired using the 647 nm excitation laser (160 mW, 1.9 kW/cm^2). Upon laser excitation, fluorescence was collected by a 100x 1.49 NA oil-immersion objective, passed through a quad-band dichroic mirror (97335 Nikon), and detected by a Hamamatsu ORCA Flash 4.0 CMOS camera with 160 nm pixel size. The signal was collected using the following settings: 512x512 pixel region, no binning, pixel depth 16-bit, exposure time 50 ms, live-cell observation and 2D-STORM (lens out), zoom 1x, lens x0.4, and for live-cell observation at 37 °C the correction collar was set to position 8160.

Acquisition of Glyco-PAINT recordings 5×10^4 CHO-MR, 1×10^5 BMDC or BMDM were seeded in 8-well glass-bottomed microscopy slides (Ibidi, 80827) in complete medium. After equilibration in the microscope incubator, fluorescent glycan was added at 5 nM for CHO-MR and 10 nM for BMDC or BMDM experiments. Then, cells were brought into focus using brightfield illumination and 2,000 frames (at 50 ms intervals) were recorded within a single field-of-view at 40–60% of maximum 647 nm laser power using TIRF illumination. For indicated experiments, Cytochalasin D (Focus Biomolecules) was added to a final concentration of 10 μ M for 30 min prior to acquisition.

Glyco-PAINT-APP analysis of recordings Processing of recordings using Glyco-PAINT-APP was performed as described in a step-by-step procedure in the Supplementary Manual and accompanying Supplementary Videos 1 and 2 that are available through GitHub. For the TrackMate processing, a batch file (Experiment Info.csv) containing the experiment metadata and tracking parameters was created. Threshold values were set to 5, 10 or 15 such that no more than 1,500,000 spots were detected. Recordings were then processed in TrackMate using the ‘Run TrackMate Batch’ plugin provided by the Glyco-PAINT-APP. Spot detection and tracking by TrackMate was performed as indicated in the batch file using the Simple LAP tracker algorithm with a maximum frame gap of 3, a max linking distance of 0.6 μ m and a gap closing max distance of 1.2 μ m. Tracks with only two spots were discarded. For the parameter sensitivity analysis, each tracking or spot detection was varied as indicated whilst the others were kept at the aforementioned values (basis scenario).

With the Glyco-PAINT-APP utility ‘Generate Squares’, a grid of squares was overlaid and kinetic properties for each square were calculated. Default parameters for grid processing are (deviations are mentioned in figure captions): Nr of Squares in row 20, Minimum Tracks to Calculate Tau 20, Min allowable R Squared 0.1, Min Required Density Ratio 2, Maximum Allowable Variability 10 and Neighbour Mode Free. For every recording, a background track count was calculated by averaging the track count of the 40 (10% of the total number of squares) least dense squares. Only squares for which the track count exceeded the Min Required Density Ratio of 2 were considered. For each square, the variability was calculated and only squares for which the variability was less than the Maximum Allowable Variability of 10 were considered. For squares meeting both the Minimum Required Density Ratio and Maximum Allowable Variability criteria, and containing at least the Minimum Tracks to Calculate Tau, kinetic parameters including k_{on} , k_{off} and MSD were calculated as in Riera *et al.*³¹, or copied from the TrackMate Tracks table output (for velocity, displacement, and track duration). Summary files were created using the ‘Compile Project’ utility, creating an ‘All Recordings.csv’ file an ‘All Squares.csv’ file, and an ‘All Tracks.csv’ file. Statistical analysis and plotting using these merged files was performed using the `ggplot2` package in R.^{52,53}

3.4. Methods

Spatial Clustering Analysis Spatial clustering of single-molecule tracks was quantified as $L(r) - r \Big|_{r=2\mu\text{m}}$ from Ripley's L-function, computed using `spatstat.explore` and `spatstat.geom` packages in R on filtered x/y track coordinates from pre-selected squares, with differences between adjuvant conditions assessed by pairwise Wilcoxon tests with Benjamini–Hochberg correction.

3.5. Supplementary Figures

Figure S3.1: Synthetic scheme for glycopeptides 1–7. Black circle represents Tentagel S RAM resin. Reagents and conditions: (a) SPPS (HCTU, Fmoc-TEG-OH, Fmoc-Lys(N₃)-OH) b) i) 20% (v/v) piperidine/DMF ii) Ac₂O, DiPEA, DMF c) i) AcOH, TFE, DCM ii) Et₃N, DMF iii) sCy5-COOH, HCTU, DiPEA, DMF d) i) TFA, TIS, H₂O ii) RP-HPLC e) i) **14** or **15**, CuSO₄, NaAsc, THPTA, DMSO, 40 °C ii) SEC. Synthetic procedures have been described for propargyl mannosides **14** and **15** by Riera *et al.*³¹ and Hogervorst and Li *et al.*²⁴ respectively.

Chapter 3. Correlating mannose binding to myeloid cell function

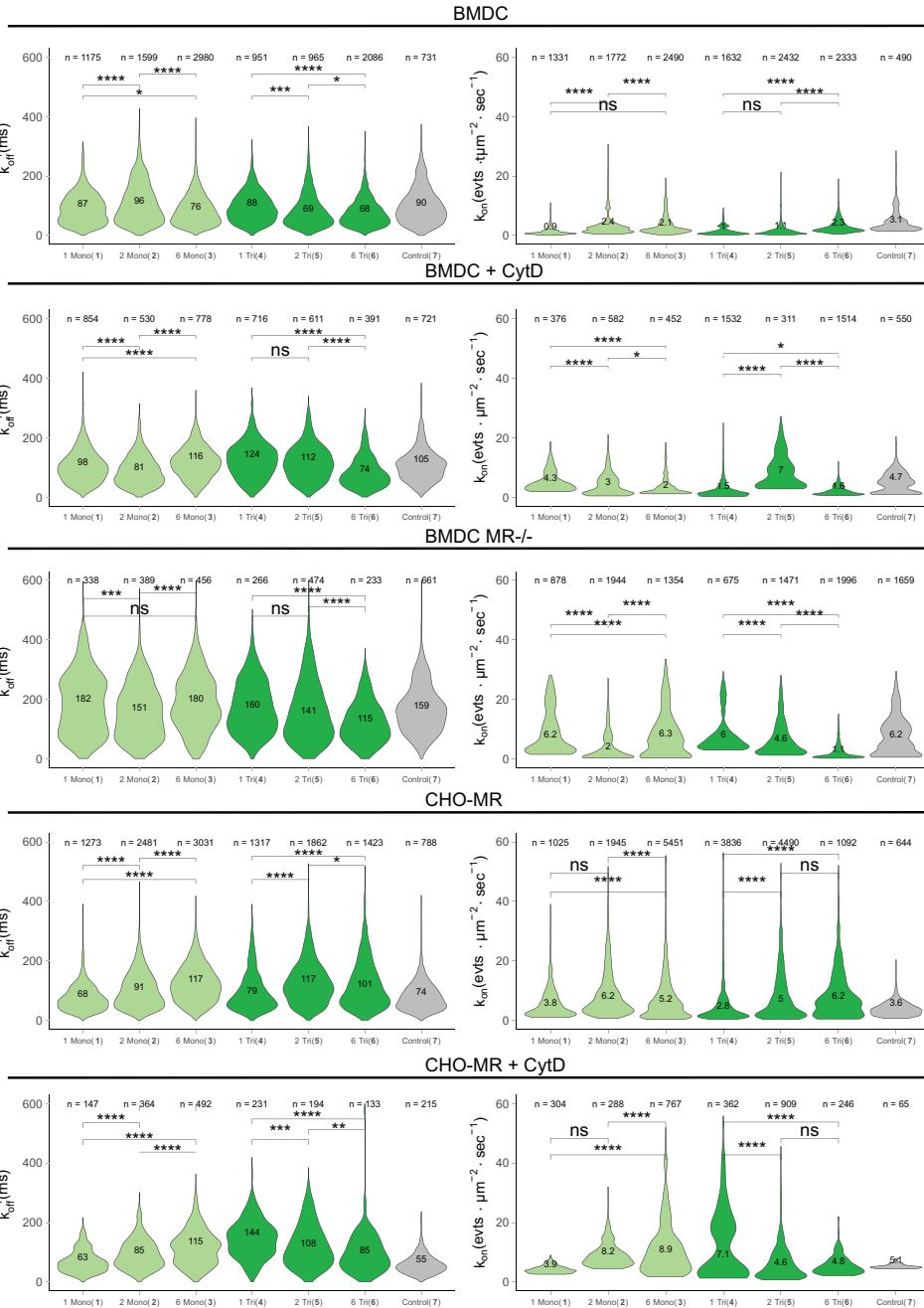


Figure S3.2

3.5. Supplementary Figures

Figure S3.2: Violin distribution of Glyco-PAINT-APP derived k_{on} and k_{off}^{-1} for glycan SLP 1-7 binding to BMDC, BMDC MR^{-/-} and CHO-MR. Square selection criteria as in **Figure 3.2**. n_i indicates the number of squares that were selected per violin. Significance across probes of similar glycan structure was assessed using two-way ANOVA followed by a Tukey post-hoc test.

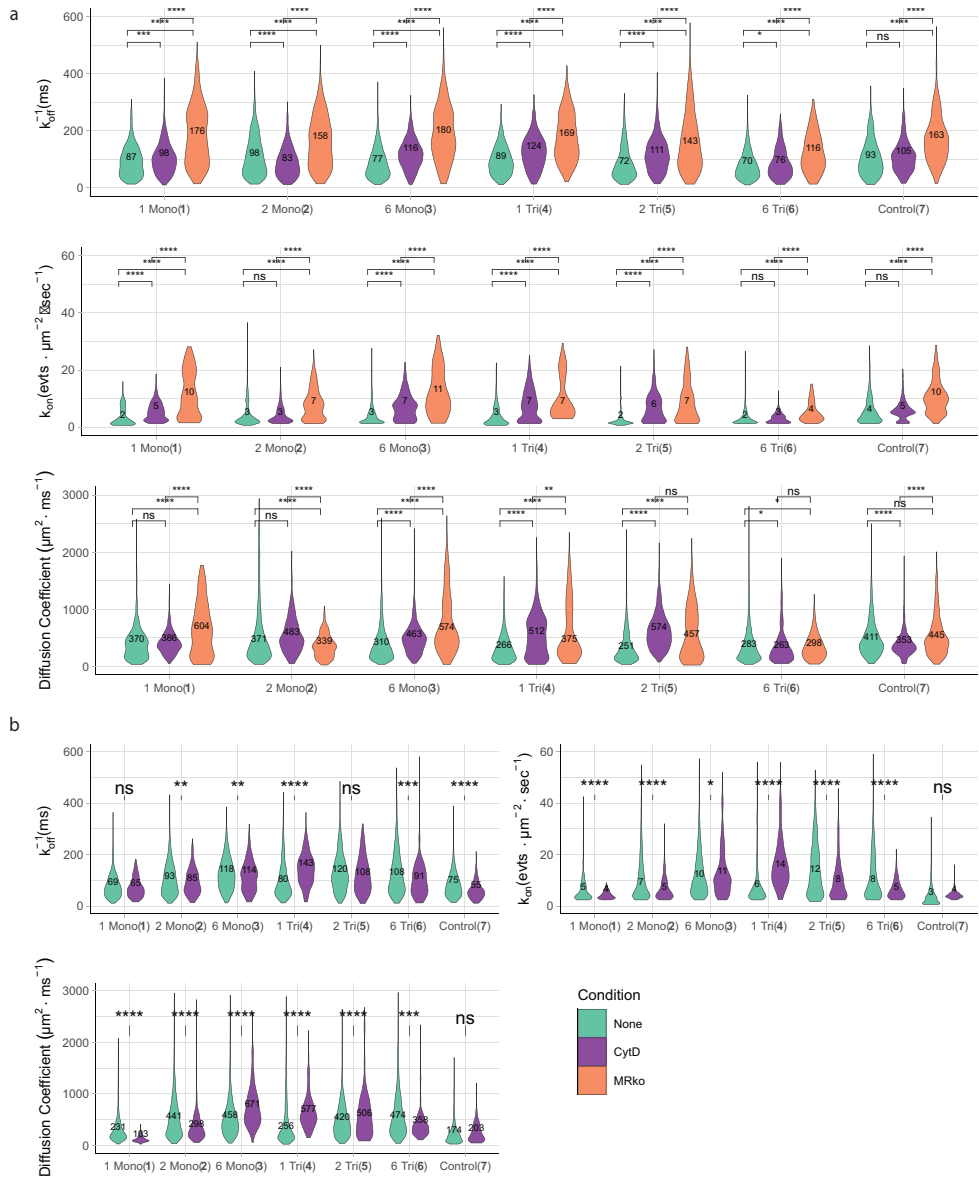


Figure S3.3: Violin distribution of Glyco-PAINT-APP derived k_{on} and k_{off}^{-1} for glycan SLP 1-7 binding to BMDC, BMDC MR^{-/-} and CHO-MR treated with CytD. (a) BMDC and (b) CHO-MR, legend is shared between a and b. Square selection criteria as in main Figure 3.2. n, indicates the number of squares that were selected per violin. Significance across cell types or CytD treatment was assessed using two-way ANOVA followed by a Tukey post-hoc test.

3.5. Supplementary Figures

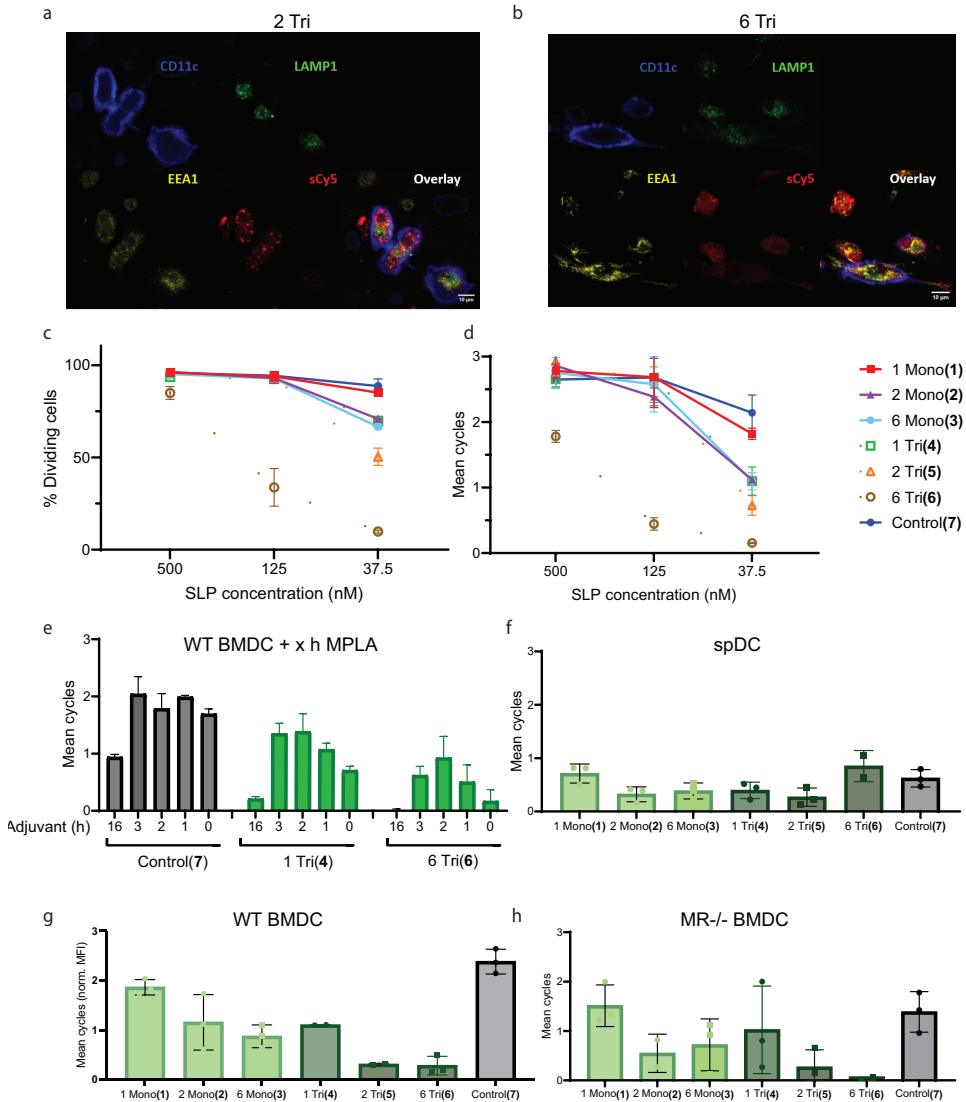


Figure S3.4: Uptake and cross-presentation of 1-7. (a, b) Confocal imaging of glycan SLP uptake by BMDC. Cells were pulsed for 1 h with 250 nM 5 or 6 after being fixed and permeabilized and then stained for CD11c, EEA1 and LAMP1 using fluorophore labeled antibodies. (c, d) Cross-presentation by BMDC pulsed with different concentrations of antigen 1-7. Amounts of cross-presentation were determined by flow cytometric measurement of CFSE-dilution by proliferating cognate T cells and quantified using mean cycle or percentage dividing cells of DMSO. (e) Pretreatment of BMDC with 1 μ g/mL MPLA for indicated time before 2h pulse with antigen 1-7 and 3d coculture with OT-I cells. (f) Cross-presentation of antigens 1-7 by magnetically purified splenic DC. (g) Cross-presentation of immature BMDC pulsed with SLPs 1-7. (h) Cross-presentation of BMDC MR^{-/-} pulsed with SLPs 1-7.

Chapter 3. Correlating mannose binding to myeloid cell function

Table 3.1: Median GlycoPAINT-APP-derived binding and mobility parameters for probe 1–7 binding to BMDC, BMDC MR^{-/-} and CHO-MR. Square selection criteria as in Fig. Figure 3.2a,b. Cells were treated with 10 μ M Cytochalasin D for 30 min where indicated. τ , characteristic binding lifetime; TTD, total track duration; LTD, long track duration; STD, short track duration; DC, diffusion coefficient. Conventional units for each parameter can be found in Table 2.1.

Cell Type	Adjuvant	Probe	Tau (τ)	Density	TTD	LTD	STD	DC	Speed	Max Speed
CHO-MR	None	1 Mono	69	4.7	17.7	1.55	0.1	231	2.1	3.2
CHO-MR	None	2 Mono	93	7.5	28.5	1.52	0.1	441	2.3	4.5
CHO-MR	None	6 Mono	118	9.7	35.5	1.43	0.1	458	2.1	4.5
CHO-MR	None	1 Tri	80	5.7	21.4	1.55	0.1	256	1.7	3.2
CHO-MR	None	2 Tri	120	11.9	43.0	1.40	0.1	420	1.9	3.2
CHO-MR	None	6 Tri	108	8.1	34.1	1.80	0.1	474	2.3	4.5
CHO-MR	None	Control	75	2.9	16.8	1.30	0.1	174	1.6	3.2
CHO-MR	CytD	1 Mono	65	3.8	9.9	1.00	0.1	103	1.6	3.2
CHO-MR	CytD	2 Mono	85	5.2	15.9	1.02	0.1	298	2.2	4.5
CHO-MR	CytD	6 Mono	114	10.6	32.6	1.15	0.1	671	2.6	4.5
CHO-MR	CytD	1 Tri	143	14.3	51.6	1.30	0.1	577	2.6	4.5
CHO-MR	CytD	2 Tri	108	7.8	32.3	1.40	0.1	506	2.3	4.5
CHO-MR	CytD	6 Tri	91	5.5	15.4	0.90	0.1	358	2.4	4.5
CHO-MR	CytD	Control	55	4.0	11.8	1.15	0.1	203	2.3	4.5
BMDC	None	1 Mono	87	2.3	22.5	1.15	0.1	370	2.2	4.5
BMDC	None	2 Mono	98	2.7	33.5	1.70	0.1	371	2.5	4.5
BMDC	None	6 Mono	77	2.8	22.6	1.65	0.1	310	2.1	4.5
BMDC	None	1 Tri	89	2.5	24.4	1.27	0.1	266	1.6	3.2
BMDC	None	2 Tri	72	1.7	17.5	1.65	0.1	251	1.9	3.2
BMDC	None	6 Tri	70	2.3	18.3	1.55	0.1	283	2.1	4.5
BMDC	None	Control	93	4.3	24.4	1.18	0.1	411	2.4	4.5
BMDC	CytD	1 Mono	98	4.9	25.8	1.00	0.1	386	2.1	3.2
BMDC	CytD	2 Mono	83	2.9	20.4	1.23	0.1	483	2.7	4.5
BMDC	CytD	6 Mono	116	6.9	36.9	1.00	0.1	463	2.3	4.5
BMDC	CytD	1 Tri	124	7.2	42.1	1.15	0.1	512	2.3	4.5
BMDC	CytD	2 Tri	111	5.8	34.2	1.12	0.1	574	2.7	4.5
BMDC	CytD	6 Tri	76	2.7	16.6	1.25	0.1	263	2.1	4.5
BMDC	CytD	Control	105	5.5	30.6	1.10	0.1	353	2.1	3.9
BMDC MR ^{-/-}	None	1 Mono	176	10.0	94.6	1.95	0.1	604	1.8	4.5
BMDC MR ^{-/-}	None	2 Mono	158	7.4	63.7	1.70	0.1	339	1.6	3.2
BMDC MR ^{-/-}	None	6 Mono	180	10.7	101.7	1.90	0.1	574	1.9	4.5
BMDC MR ^{-/-}	None	1 Tri	169	7.3	65.6	1.75	0.1	375	1.6	3.2
BMDC MR ^{-/-}	None	2 Tri	143	6.9	57.5	1.80	0.1	457	1.9	4.5
BMDC MR ^{-/-}	None	6 Tri	116	4.2	31.4	1.70	0.1	298	1.6	3.2
BMDC MR ^{-/-}	None	Control	163	9.8	84.9	1.82	0.1	445	1.6	3.2

3.5. Supplementary Figures

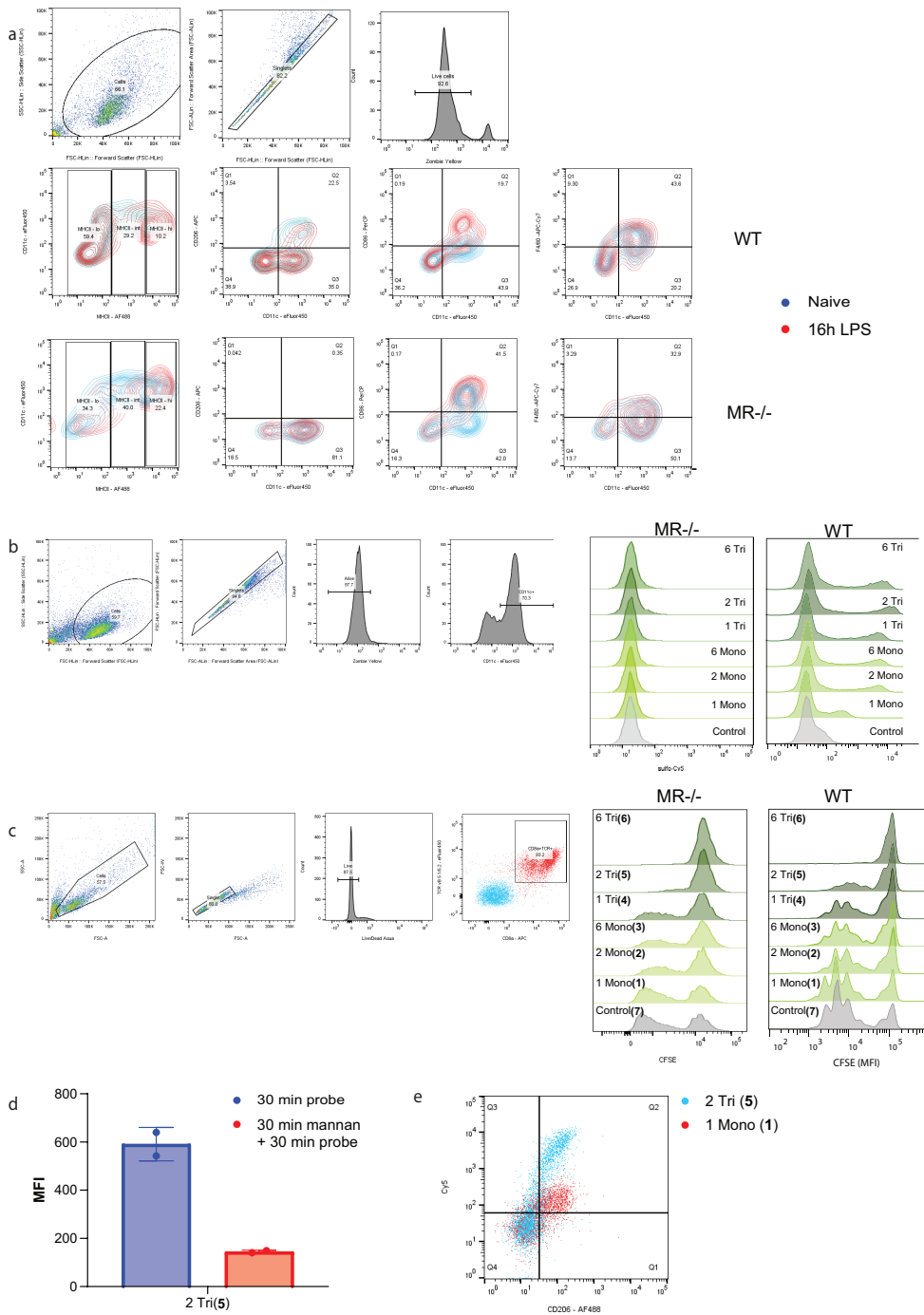


Figure S3.5

Chapter 3. Correlating mannose binding to myeloid cell function

Figure S3.5: Flow cytometry assays for uptake and cross-presentation of glycan SLP 1–7 (a) Characterization of BMDC WT and MR^{-/-} cell surface marker expression and functional response to 100 ng/mL LPS stimulation for 16 h by flow cytometry. Shown is the gating strategy and expression profiles of CD11c, MHCII, CD206, CD86 and F4-80. (b) Gating strategy for glycan uptake experiments in BMDC WT and MR^{-/-}. (c) Same as in **b** for OT-I T cell proliferation experiments. (d) Endocytosis of **5** is blocked by pre-incubation of BMDC with 2 mg/mL mannan for 30 min. (e) Mannosylated antigens **1** and **5** are taken up by CD11c⁺CD206⁺ BMDC.

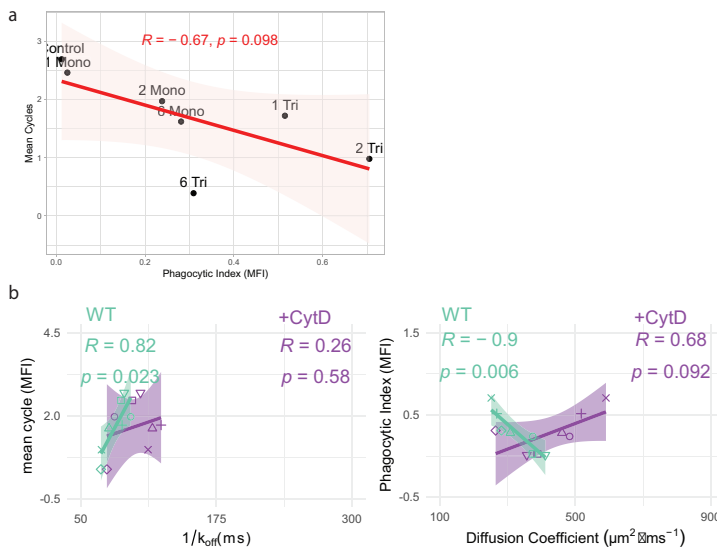


Figure S3.6: Correlation between phagocytic index, T cell proliferation and Glyco-PAINT-APP kinetics 1-7 to BMDC binding. (a) Glycan uptake and T cell proliferation (mean cycle) correlation. (b) Correlation analysis of Glycan SLP functionality (T cell proliferation and uptake) with k_{off}^{-1} and diffusion coefficients as determined by Glyco-PAINT-APP for untreated or CytD treated BMDC. Pearson's R and two-tailed t test P value are displayed in the correlation plots.

3.5. Supplementary Figures

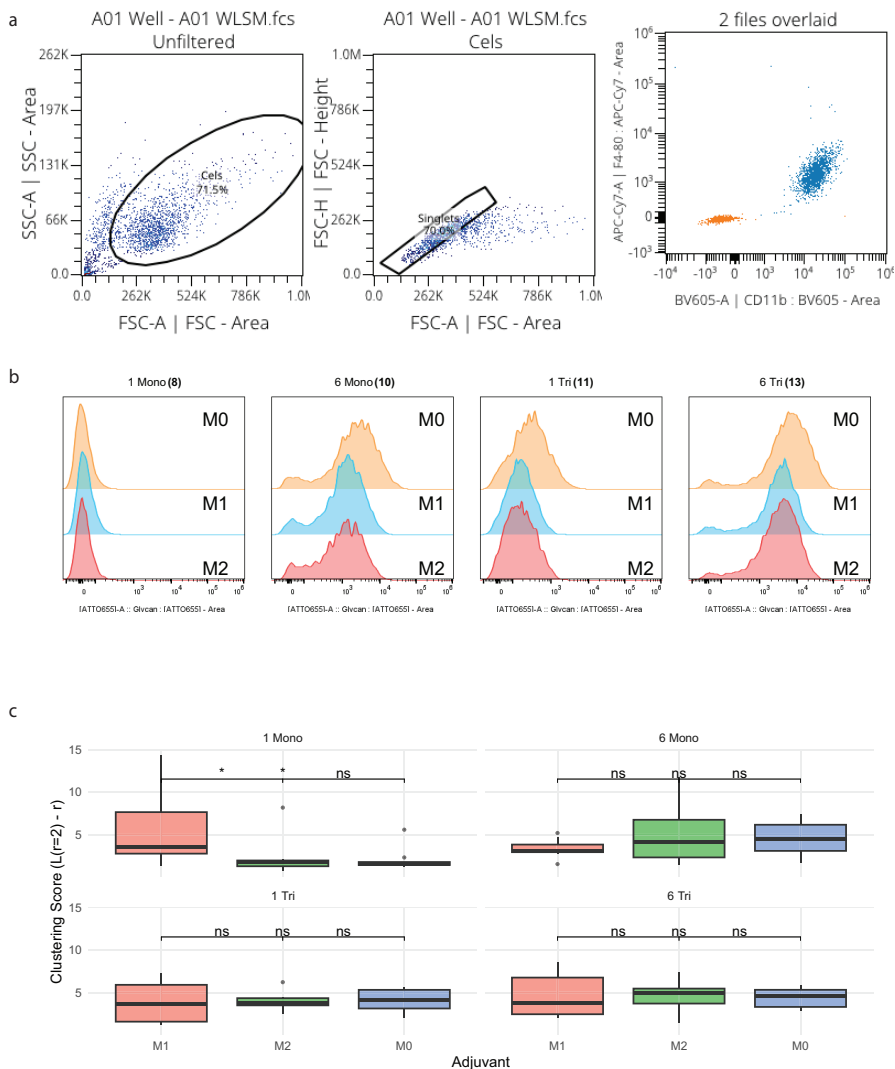


Figure S3.7: Glycan uptake and clustering of binding events by macrophages. (a) Gating strategy for flow cytometric quantification of glycan 8, 10, 11 or 13 uptake by BMDM. (b) Flow cytometry histograms of relative uptake of glycans by BMDM treated with M0-2 polarization stimuli. (c) Clustering analysis of Glyco-PAINT-APP binding events on polarizing macrophages. Clustering score was determined using Ripley-K clustering algorithm with r (radius) of $1 \mu\text{m}$. See experimental methods for further details regarding clustering analysis.

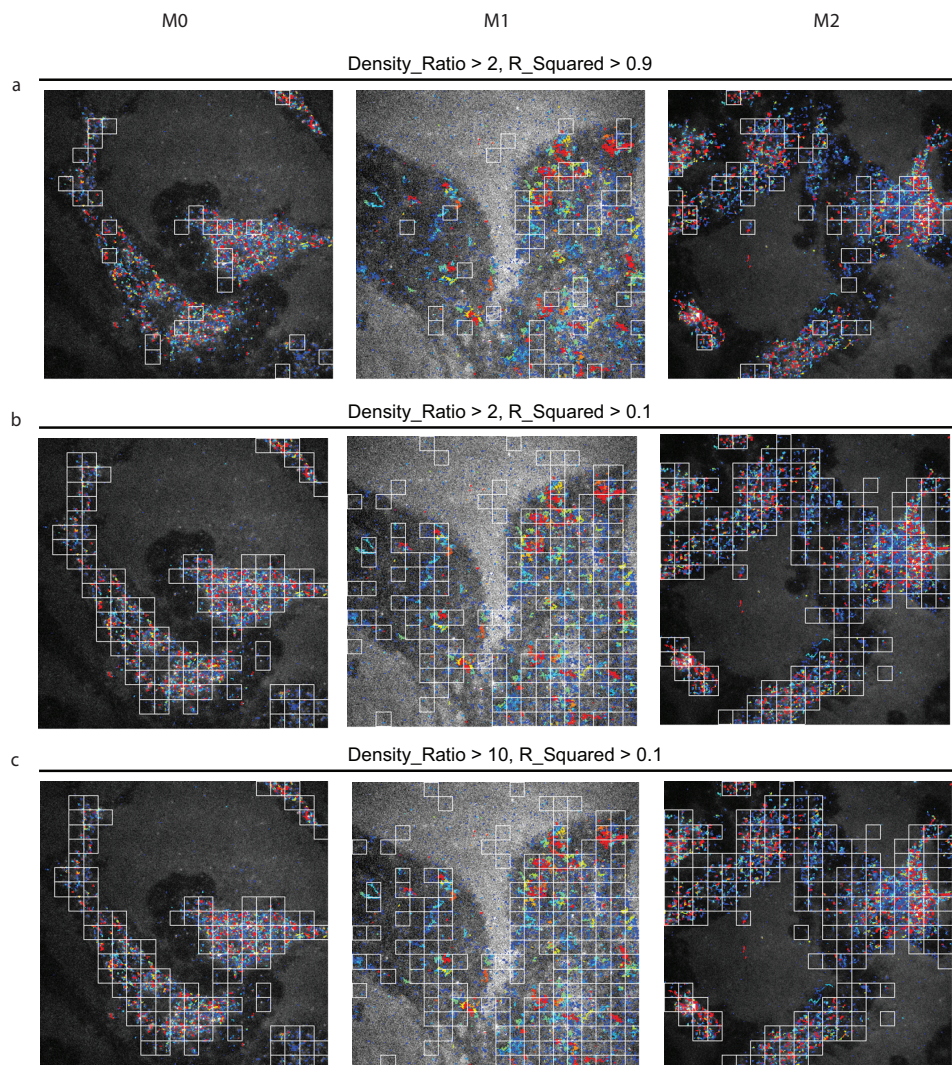


Figure S3.8: Square selection criteria for macrophages. Identical recordings of glycan 8 binding to M0, M1 and M2 macrophages with varying Density_Ratio and R_Squared selection criteria set to R_Squared > 0.9 (standard) in (a), R_Squared > 0.1 in (b) or Density_Ratio > 10 in (c).

References

- (1) *Essentials of Glycobiology*, 4th; Varki, A., Cummings, R. D., Esko, J. D., Stanley, P., Hart, G. W., Aebi, M., Mohnen, D., Kinoshita, T., Packer, N. H., Prestegard, J. H., Schnaar, R. L., Seeberger, P. H., Eds.; Cold Spring Harbor Laboratory Press: Cold Spring Harbor (NY), 2022.
- (2) Sousa, C. R. e.; Yamasaki, S.; Brown, G. D. Myeloid C-type lectin receptors in innate immune recognition. *Immunity* **2024**, *57*, 700–717.
- (3) Marth, J. D.; Grewal, P. K. Mammalian glycosylation in immunity. *Nature Reviews Immunology* **2008**, *8*, 874–887.
- (4) Van der Zande, H. J. P.; Nitsche, D.; Schlautmann, L.; Guigas, B.; Burgdorf, S. The Mannose Receptor: From Endocytic Receptor and Biomarker to Regulator of (Meta)Inflammation. *Frontiers in Immunology* **2021**, *12*, 765034.
- (5) Stahl, P. D.; Rodman, J. S.; Miller, M. J.; Schlesinger, P. H. Evidence for receptor-mediated binding of glycoproteins, glycoconjugates, and lysosomal glycosidases by alveolar macrophages. *Proceedings of the National Academy of Sciences* **1978**, *75*, 1399–1403.
- (6) Stahl, P. D.; Ezekowitz, R. A. B. The mannose receptor is a pattern recognition receptor involved in host defense. *Current opinion in immunology* **1998**, *10*, 50–55.
- (7) Brown, G. D.; Willment, J. A.; Whitehead, L. C-type lectins in immunity and homeostasis. *Nature Reviews Immunology* **2018**, *18*, 374–389.
- (8) Taylor, P. R.; Gordon, S.; Martinez-Pomares, L. The mannose receptor: linking homeostasis and immunity through sugar recognition. *Trends in Immunology* **2005**, *26*, 104–110.
- (9) Feinberg, H.; Jégouzo, S. A. F.; Lasanajak, Y.; Smith, D. F.; Drickamer, K.; Weis, W. I.; Taylor, M. E. Structural analysis of carbohydrate binding by the macrophage mannose receptor CD206. *Journal of Biological Chemistry* **2021**, *296*.
- (10) Solinas, G.; Schiarea, S.; Liguori, M.; Fabbri, M.; Pesce, S.; Zammataro, L.; Pasqualini, F.; Nebuloni, M.; Chiabrando, C.; Mantovani, A.; Allavena, P. Tumor-Conditioned Macrophages Secrete Migration-Stimulating Factor: A New Marker for M2-Polarization, Influencing Tumor Cell Motility. *The Journal of Immunology* **2010**, *185*, 642–652.
- (11) Schuette, V. et al. Mannose receptor induces T-cell tolerance via inhibition of CD45 and up-regulation of CTLA-4. *Proceedings of the National Academy of Sciences* **2016**, *113*, 10649–10654.
- (12) Mastrotto, F.; Pirazzini, M.; Negro, S.; Salama, A.; Martinez-Pomares, L.; Mantovani, G. Sulfation at Glycopolymer Side Chains Switches Activity at the Macrophage Mannose Receptor (CD206) In Vitro and In Vivo. *Journal of the American Chemical Society* **2022**, *144*, 23134–23147.
- (13) Martinez-Pomares, L. The mannose receptor. *Journal of Leukocyte Biology* **2012**, *92*, 1177–1186.
- (14) Napper, C. E.; Drickamer, K.; Taylor, M. E. Collagen binding by the mannose receptor mediated through the fibronectin type II domain. *Biochemical Journal* **2006**, *395*, 579–586.
- (15) Mullin, N. P.; Hitchen, P. G.; Taylor, M. E. Mechanism of Ca²⁺- and Monosaccharide Binding to a C-type Carbohydrate-recognition Domain of the Macrophage Mannose Receptor *. *Journal of Biological Chemistry* **1997**, *272*, 5668–5681.
- (16) Stavenhagen, K.; Mehta, A. Y.; Laan, L.; Gao, C.; Heimburg-Molinaro, J.; van Die, I.; Cummings, R. D. N-glycosylation of mannose receptor (CD206) regulates glycan binding by C-type lectin domains. *The Journal of Biological Chemistry* **2022**, *298*, 102591.

- (17) Geijtenbeek, T. B. H.; Gringhuis, S. I. Signalling through C-type lectin receptors: shaping immune responses. *Nature Reviews Immunology* **2009**, *9*, 465–479.
- (18) Schweizer, A.; Stahl, P. D.; Rohrer, J. A di-aromatic motif in the cytosolic tail of the mannose receptor mediates endosomal sorting. *The Journal of Biological Chemistry* **2000**, *275*, 29694–29700.
- (19) Rajaram, M. V.; Arnett, E.; Azad, A. K.; Guirado, E.; Ni, B.; Gerberick, A. D.; He, L.-Z.; Keler, T.; Thomas, L. J.; Lafuse, W. P.; Schlesinger, L. S. M. tuberculosis-initiated human mannose receptor signaling temporally regulates macrophage recognition and vesicle trafficking by FcR γ -chain, Grb2 and SHP-1. *Cell reports* **2017**, *21*, 126–140.
- (20) Kang, P. B.; Azad, A. K.; Torrelles, J. B.; Kaufman, T. M.; Beharka, A.; Tibesar, E.; DesJardin, L. E.; Schlesinger, L. S. The human macrophage mannose receptor directs Mycobacterium tuberculosis lipoarabinomannan-mediated phagosome biogenesis. *The Journal of Experimental Medicine* **2005**, *202*, 987–999.
- (21) Burgdorf, S.; Kurts, C. Endocytosis mechanisms and the cell biology of antigen presentation. *Current Opinion in Immunology* **2008**, *20*, 89–95.
- (22) Burgdorf, S.; Kautz, A.; Böhnert, V.; Knolle, P. A.; Kurts, C. Distinct Pathways of Antigen Uptake and Intracellular Routing in CD4 and CD8 T Cell Activation. *Science* **2007**, *316*, 612–616.
- (23) Hogervorst, T. P.; Li, R. J. E.; Marino, L.; Bruijns, S. C. M.; Meeuwenoord, N. J.; Filippov, D. V.; Overkleef, H. S.; van der Marel, G. A.; van Vliet, S. J.; van Kooyk, Y.; Codée, J. D. C. C - Mannosyl Lysine for Solid Phase Assembly of Mannosylated Peptide Conjugate Cancer Vaccines. *ACS Chemical Biology* **2020**, *15*, 728–739.
- (24) Li, R.-J. E. et al. Systematic Dual Targeting of Dendritic Cell C-Type Lectin Receptor DC-SIGN and TLR7 Using a Trifunctional Mannosylated Antigen. *Frontiers in Chemistry* **2019**, *7*, 650.
- (25) McIntosh, J. D.; Brimble, M. A.; Brooks, A. E. S.; Dunbar, P. R.; Kowalczyk, R.; Tomabechi, Y.; Fairbanks, A. J. Convergent chemo-enzymatic synthesis of mannosylated glycopeptides; targeting of putative vaccine candidates to antigen presenting cells. *Chemical Science* **2015**, *6*, 4636–4642.
- (26) Segura, E.; Albiston, A. L.; Wicks, I. P.; Chai, S. Y.; Villadangos, J. A. Different cross-presentation pathways in steady-state and inflammatory dendritic cells. *Proceedings of the National Academy of Sciences* **2009**, *106*, 20377–20381.
- (27) Segura, E.; Gupta, N.; Albiston, A. L.; Wicks, I. P.; Chai, S. Y.; Villadangos, J. A. Reply to Burgdorf et al.: The mannose receptor is not involved in antigen cross-presentation by steady-state dendritic cells. *Proceedings of the National Academy of Sciences* **2010**, *107*.
- (28) Burgdorf, S.; Schuette, V.; Semmling, V.; Hochheiser, K.; Lukacs-Kornek, V.; Knolle, P. A.; Kurts, C. Steady-state cross-presentation of OVA is mannose receptor-dependent but inhibitable by collagen fragments. *Proceedings of the National Academy of Sciences* **2010**, *107*.
- (29) Singh, S. K.; Streng-Ouwehand, I.; Litjens, M.; Kalay, H.; Burgdorf, S.; Saeland, E.; Kurts, C.; Unger, W. W.; van Kooyk, Y. Design of neo-glycoconjugates that target the mannose receptor and enhance TLR-independent cross-presentation and Th1 polarization. *European Journal of Immunology* **2011**, *41*, 916–925.
- (30) Rauen, J.; Kreer, C.; Paillard, A.; van Duikeren, S.; Benckhuijsen, W. E.; Camps, M. G.; Valentijn, A. R. P. M.; Ossendorp, F.; Drijfhout, J. W.; Arens, R.; Burgdorf, S. Enhanced Cross-Presentation and Improved CD8⁺ T Cell Responses after Mannosylation of Synthetic Long Peptides in Mice. *PLoS ONE* **2014**, *9*, ed. by Kassiotis, G., e103755.
- (31) Riera, R.; Hogervorst, T. P.; Doelman, W.; Ni, Y.; Pujals, S.; Bolli, E.; Codée, J. D. C.; van Kasteren, S. I.; Albertazzi, L. Single-molecule imaging of glycan–lectin interactions on cells with Glyco-PAINT. *Nature Chemical Biology* **2021**, *17*, 1281–1288.

REFERENCES

- (32) Hogquist, K. A.; Jameson, S. C.; Heath, W. R.; Howard, J. L.; Bevan, M. J.; Carbone, F. R. T cell receptor antagonist peptides induce positive selection. *Cell* **1994**, *76*, 17–27.
- (33) Rosalia, R. A. et al. Dendritic cells process synthetic long peptides better than whole protein, improving antigen presentation and T-cell activation. *European Journal of Immunology* **2013**, *43*, 2554–2565.
- (34) Streng-Ouwehand, I.; Ho, N. I.; Litjens, M.; Kalay, H.; Boks, M. A.; Cornelissen, L. A.; Kaur Singh, S.; Saeland, E.; Garcia-Vallejo, J. J.; Ossendorp, F. A.; Unger, W. W.; van Kooyk, Y. Glycan modification of antigen alters its intracellular routing in dendritic cells, promoting priming of T cells. *eLife* **2016**, *5*, ed. by Krzych, U., e11765.
- (35) Tornøe, C. W.; Christensen, C.; Meldal, M. Peptidotriazoles on Solid Phase: [1,2,3]-Triazoles by Regiospecific Copper(I)-Catalyzed 1,3-Dipolar Cycloadditions of Terminal Alkynes to Azides. *The Journal of Organic Chemistry* **2002**, *67*, 3057–3064.
- (36) Rostovtsev, V. V.; Green, L. G.; Fokin, V. V.; Sharpless, K. B. A Stepwise Huisgen Cycloaddition Process: Copper(I)-Catalyzed Regioselective “Ligation” of Azides and Terminal Alkynes. *Angewandte Chemie International Edition* **2002**, *41*, 2596–2599.
- (37) Le Guével, X.; Perez Perrino, M.; Fernández, T. D.; Palomares, F.; Torres, M.-J.; Blanca, M.; Rojo, J.; Mayorga, C. Multivalent Glycosylation of Fluorescent Gold Nanoclusters Promotes Increased Human Dendritic Cell Targeting via Multiple Endocytic Pathways. *ACS Applied Materials & Interfaces* **2015**, *7*, 20945–20956.
- (38) Khalil, I. A.; Kogure, K.; Akita, H.; Harashima, H. Uptake Pathways and Subsequent Intracellular Trafficking in Nonviral Gene Delivery. *Pharmacological Reviews* **2006**, *58*, 32–45.
- (39) Park, Y.; Abihssira-García, I. S.; Thalmann, S.; Wiegertjes, G. F.; Barreda, D. R.; Olsvik, P. A.; Kiron, V. Imaging Flow Cytometry Protocols for Examining Phagocytosis of Microplastics and Bioparticles by Immune Cells of Aquatic Animals. *Frontiers in Immunology* **2020**, *11*.
- (40) Kimura, T. et al. Polarization of M2 macrophages requires Lamtor1 that integrates cytokine and amino-acid signals. *Nature Communications* **2016**, *7*, 13130.
- (41) Stein, M.; Keshav, S.; Harris, N.; Gordon, S. Interleukin 4 potently enhances murine macrophage mannose receptor activity: a marker of alternative immunologic macrophage activation. *The Journal of Experimental Medicine* **1992**, *176*, 287–292.
- (42) Canton, J. Macropinocytosis: New Insights Into Its Underappreciated Role in Innate Immune Cell Surveillance. *Frontiers in Immunology* **2018**, *9*.
- (43) Liu, Z.; Roche, P. A. Macropinocytosis in phagocytes: regulation of MHC class-II-restricted antigen presentation in dendritic cells. *Frontiers in Physiology* **2015**, *6*, 1.
- (44) Norbury, C. C.; Hewlett, L. J.; Prescott, A. R.; Shastri, N.; Watts, C. Class I MHC presentation of exogenous soluble antigen via macropinocytosis in bone marrow macrophages. *Immunity* **1995**, *3*, 783–791.
- (45) Watts, C.; West, M. A.; Zaru, R. TLR signalling regulated antigen presentation in dendritic cells. *Current Opinion in Immunology* **2010**, *22*, 124–130.
- (46) Chatterjee, B.; Smed-Sörensen, A.; Cohn, L.; Chalouni, C.; Vandlen, R.; Lee, B.-C.; Widger, J.; Keler, T.; Delamare, L.; Mellman, I. Internalization and endosomal degradation of receptor-bound antigens regulate the efficiency of cross presentation by human dendritic cells. *Blood* **2012**, *120*, 2011–2020.
- (47) Lee, S. J.; Evers, S.; Roeder, D.; Parlow, A. F.; Risteli, J.; Risteli, L.; Lee, Y. C.; Feizi, T.; Langen, H.; Nussenzweig, M. C. Mannose Receptor-Mediated Regulation of Serum Glycoprotein Homeostasis. *Science* **2002**, *295*, 1898–1901.

Chapter 3. Correlating mannose binding to myeloid cell function

- (48) Marim, F. M.; Silveira, T. N.; Jr, D. S. L.; Zamboni, D. S. A Method for Generation of Bone Marrow-Derived Macrophages from Cryopreserved Mouse Bone Marrow Cells. *PLOS ONE* **2010**, *5*, e15263.
- (49) Martinez-Pomares, L.; Reid, D. M.; Brown, G. D.; Taylor, P. R.; Stillion, R. J.; Linehan, S. A.; Zamze, S.; Gordon, S.; Wong, S. Y. Analysis of mannose receptor regulation by IL-4, IL-10, and proteolytic processing using novel monoclonal antibodies. *Journal of Leucocyte Biology* **2003**, *73*, 604–613.
- (50) Doelman, W. Synthetic peptides as tools in chemical immunology, en, Ph.D. Thesis, Leiden University, 2023.
- (51) Valente, M.; Baey, C.; Louche, P.; Dutertre, C.-A.; Vimeux, L.; Marañón, C.; Hosmalin, A.; Feuillet, V. Apoptotic cell capture by DCs induces unexpectedly robust autologous CD4⁺ T \square cell responses. *European Journal of Immunology* **2014**, *44*, 2274–2286.
- (52) R Core Team, *R: A Language and Environment for Statistical Computing*; R Foundation for Statistical Computing: Vienna, Austria, 2023.
- (53) Wickham, H., *ggplot2: Elegant Graphics for Data Analysis*; Springer-Verlag New York: 2016.